Generating nearly single-cycle pulses with increased intensity and strongly asymmetric pulses of petawatt level

Inhyuk Nam,[1] Victor V. Kulagin,[2,*] Min Sup Hur,[3] In Won Lee,[4] and Hyyong Suk[1,4,†]

[1]*Department of Photonics and Applied Physics, Gwangju Institute of Science and Technology (GIST), Gwangju 500-712, Korea*
[2]*Sternberg Astronomical Institute, Moscow State University, Moscow 119992, Russia*
[3]*School of Electrical and Computer Engineering, Ulsan National Institute of Science and Technology (UNIST), Ulsan 689-798, Korea*
[4]*Advanced Photonics Research Institute, Gwangju Institute of Science and Technology (GIST), Gwangju 500-712, Korea*

Generation of petawatt-class pulses with a nearly single-cycle duration or with a strongly asymmetric longitudinal profile using a thin plasma layer are investigated via particle-in-cell simulations and the analytical flying mirror model. It is shown that the transmitted pulses having a duration as short as about 4 fs (1.2 laser cycles) or one-cycle front (tail) asymmetric pulses with peak intensity of about 10^{21} W/cm^2 can be produced by optimizing system parameters. Here, a new effect is found for the shaping of linearly polarized laser pulses, owing to which the peak amplitude of the transmitted pulse becomes larger than that of the incoming pulse, and intense harmonics are generated. Characteristics of the transmitting window are then studied for different parameters of laser pulse and plasma layer. For a circular polarization, it is shown that the flying mirror model developed for shaping laser pulses with ultrathin foils can be successfully applied to plasma layers having a thickness of about the laser wavelength, which allows the shape of the transmitted pulse to be analytically predicted.

PACS number(s): 52.38.−r, 42.65.Re, 52.27.Ny, 52.65.Rr

I. INTRODUCTION

Interactions of ultraintense laser pulses with thin foils have been investigated for nearly two decades [1–5]. Based on this body of research, various interesting physical phenomena have been predicted and observed in laser-foil interactions, such as the generation of high harmonics [6] and attosecond x-ray pulses [7,8], in addition to the formation of relativistic electron mirrors [9,10] and the acceleration of electrons and ions [11], among others. One of these phenomena is laser pulse shaping using ultrathin foils, first proposed in Ref. [12]. The analytical theory for the shaping was originally derived for moderate laser pulse amplitudes [1] (sliding mirror model). Later, this theory was generalized for arbitrary amplitudes of the incoming pulse [13] (flying mirror model). Shaping enables few-cycle pulses with a high intensity to be produced, which are very promising for the generation of attosecond pulses [14], the laser wakefield acceleration of monoenergetic electron bunches [15], the generation of relativistic electron mirrors [10], and coherent x-ray pulses [7,8], among other uses.

Laser pulse shaping with ultrathin foils is based on the use of relativistic nonlinearity and self-induced transparency [16–22], which is induced by a field having an amplitude $a_0 > 1$, where $a_0 = |e| E / m_e \omega_0 c$; e and m_e are the electron charge and mass, E and ω_0 are the electric field and frequency of the incident wave, and c is the speed of light in a vacuum. During this process, electrons achieve relativistic velocities in the wave, which leads to a decrease of the effective plasma frequency $\omega_{\mathrm{pef}} = \omega_p/\sqrt{\gamma}$, where γ is the average relativistic factor of the electrons and $\omega_p = \sqrt{4\pi n e^2/m}$; n is the electron density. This means that for ultrathin foils having a thickness

considerably smaller than the laser wavelength, the part of the laser pulse having moderate intensity is reflected and the high-intensity part is transmitted. Recently, it was shown that a nearly single-cycle pulse can be generated via the interaction of an ultraintense circularly polarized laser pulse with a thin foil [23]; however, the decrease of the maximal amplitude was about 40%. An alternative way is to use an ultrafast-ionization shuttering for shaping laser pulses [24]. Few-cycle laser pulses can be also produced using an optical parametric chirped-pulse amplifier [25], though there are strong limitations on the intensity increase in this case due to damage incurred by the optical components from the ultraintense few-cycle pulse.

In this paper, using one-dimensional (1D) particle-in-cell (PIC) simulations, we show that two scenarios for shaping the laser pulse using a plasma layer can be realized. In the first scenario, the transmitting plasma window closes in a short time after inducing the transmission, thereby producing a very short (up to single-cycle duration) transmitted pulse. In the second case, the transmitting plasma window can survive until the end of the incoming laser pulse, thus producing a strongly asymmetrical transmitted pulse with a very sharp front (up to one cycle) and a relatively long tail. In this second case, the reflected pulse has a smooth front and a sharp tail. A new effect was found for shaping the laser pulses having linear polarization, which increases the transmitted pulse maximal amplitude up to that of the incoming laser pulse and even higher (in contrast to shaping circularly polarized pulses, in which the amplitude can be decreased by 40% or more). The physical process behind this effect was identified as the transfer of energy from the longitudinal oscillations of electrons (pumped by the incoming pulse front) to the transverse electric field due to coherent electron radiation and the strongly nonlinear interaction in the presence of a laser pulse field.

This interaction vastly enriches the transmitted pulse by adding intense harmonics. The characteristics of the

*victorvkulagin@yandex.ru
†hysuk@gist.ac.kr

026405-1

transmitting window are then studied for different parameters of the laser pulse and plasma layer. To shape laser pulses having a circular polarization, we show that the self-consistent flying mirror model developed earlier for ultrathin foils [13] can also be successfully applied to the case of plasma layers having a thickness of about the laser wavelength, thereby allowing the shape of the transmitted pulse to be analytically predicted. Finally, we confirm the 1D results via two-dimensional (2D) PIC simulations.

The remainder of this paper is organized as follows: Shaping laser pulses having linear polarization are presented in Sec. II. In Sec. III, results relevant for circularly polarized laser pulses are presented. Sec. IV then concludes the discussion.

II. SHAPING LASER PULSES HAVING LINEAR POLARIZATION

A. Guidelines for shaping and simulation parameters

For these simulations, a 1D version of the XOOPIC code [26] was used. The linearly y-polarized (circularly polarized) laser pulse has a Gaussian envelope with a full width at half maximum (FWHM) of $\tau_l = 5.83$ ($w_0 = 3.5$ for the $1/e$ level) and full duration of $\tau = 14$ (all times are normalized by the laser period T_0), a peak amplitude of $a_0 = 20$, and a wavelength of $\lambda_0 = 1$ μm. The pulse propagates along the x axis and has a normal incidence at the plasma layer. The plasma consists of electrons and ions with an ion mass of $m_p = 1836\,m_e$ for protons or $m_c = 12.011m_p$ for carbon ions. The thickness of the plasma layer is from $0.36\lambda_0$ to $1.2\lambda_0$, with an initial electron density n_0 from $8n_{cr}$ to $12n_{cr}$, in which all densities are normalized by the critical density $n_{cr} = m_e\,\omega_0^2\,/4\,\pi\,e^2$. Note that we used 800 grid points per λ_0 and 200 particles per cell in 1D simulations.
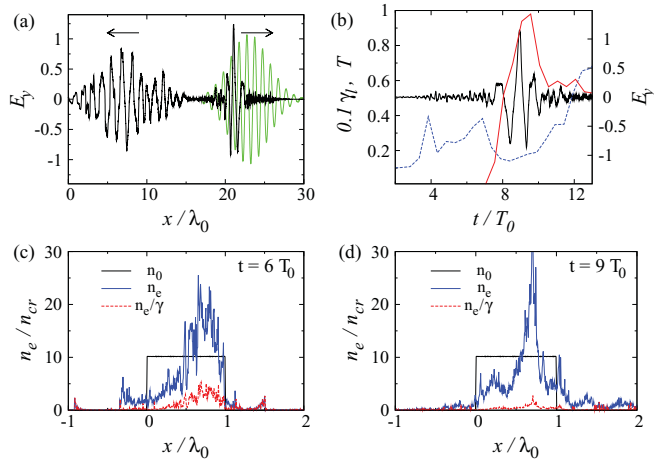

FIG. 1. (Color online) (a) Shapes of the incident laser pulse [green (light gray) line, $a_0 = 20$] and the pulse after interaction with a foil having an initial thickness $d = \lambda_0$ and $n_0 = 10n_{cr}$ (solid black line; arrows show the direction of propagation for the parts of this pulse). (b) Transmittance coefficient of the plasma layer [red (right gray) line], transmitted pulse (solid black line), and the averaged longitudinal relativistic factor of the electrons (dashed blue line). Distributions of the electron density n_e (solid blue lines) at (c) $t = 6T_0$ and (d) $t = 9T_0$ from the beginning of the interaction (dashed red lines are for effective density n_e/γ).

Let us first consider the linear polarization case. Two modes are generally possible for laser pulse penetration into a target [27]. In the first mode, referred to as the hole-boring mode [28], the electron density is so large (or the laser pulse amplitude is not high enough) that the ions generally move together with the electrons. In this case, a charged double layer is formed and a shock wave is usually launched [27,29]. The electron density can be increased by many times here, so a relatively long time is needed in order to heat the electrons. The second mode, the anomalous penetration mode [27], is realized for a moderate electron density (or high field amplitude). In this case, the ions cannot follow the electrons, and the double layer is absent. This mode is characterized by a moderate increase of the electron density and has a correspondingly shorter heating time prior to the start of transmission. According to our simulations, this mode generates transmitted pulses with shorter fronts so it is more appropriate for shaping. For this reason, in the sections below, we consider shaping only in the anomalous penetration mode.

During interaction, the front of the laser pulse compresses the electrons via a ponderomotive force, and the electron density is increased as seen in the left part of Fig. 1(c) [blue (solid gray) line]. Concurrently, electrons move violently in this region because of the Lorentz force. The large $\boldsymbol{v} \times \boldsymbol{B}$ term of this force generates a longitudinal motion and strong mixing of electrons in the fields of the incident and reflected waves. Hence, this case can be referred to as stochastic shaping. Then, the effective plasma density $n_{eff} = n_e/\gamma$ decreases [red (dashed) line in Fig. 1(c); for γ, the average of the γ values for all electrons in each cell is used] and the laser pulse propagates into the plasma layer. The penetration velocity for the laser pulse front depends on parameters such as the electron density, the amplitude and form of the laser pulse envelope, ion charge, and ion-to-electron mass ratio [27]. A more detailed study of the penetration dynamics will be presented at a later time. After some time from the beginning of the interaction, referred to as the penetration time, the laser pulse front reaches the rear boundary of the target. To make transmission possible, the maximal amplitude of the laser pulse should be sufficiently high. In this case, all electrons in the plasma layer become hot enough for n_{eff} to decrease below n_{cr}, and the plasma becomes transparent [Fig. 1(d); red (dashed) line]. The entire process usually lasts for several laser periods, so the target thickness does not increase considerably during this time.

The ion motion plays an important role in closing the transparent channel. Generally, the strong electrostatic force induced by the electron motion accelerates ions. However, if the ions are heavy, they cannot catch up with the electrons after passing the laser pulse maximum; therefore, the electron density grows up slowly, and a transparent channel exists for the total laser pulse duration. In the opposite situation, when the ions are light, they can easily follow the electron distribution and form a density peak [27]. As a result, when the laser pulse maximum passes and the laser pulse pressure decreases, the electrons return to the ions and their density increases. Finally, n_{eff} becomes greater than n_{cr}, and the transparent channel closes. The transmittance coefficient of the plasma layer (calculated as the total transmittance of all nontransparent cells, i.e., cells with $n_{eff} > n_{cr}$) is shown in Fig. 1(b) [red (solid gray) line]. The transmittance begins to
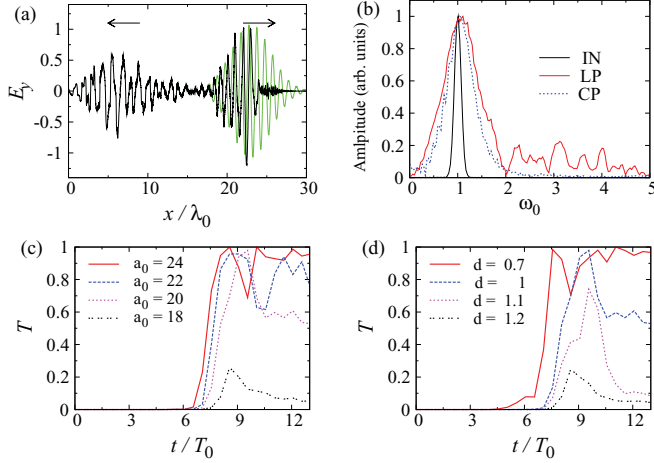
FIG. 2. (Color online) (a) The same as in Fig. 1 but for $d = 0.7\lambda_0$. (b) Spectra of the incident (IN) and the transmitted pulses having linear polarization (LP) and circular polarization (CP). The evolution of the plasma layer transmittance with (c) a field amplitude for $d = \lambda_0$, and (d) foil thickness for $a_0 = 20$.
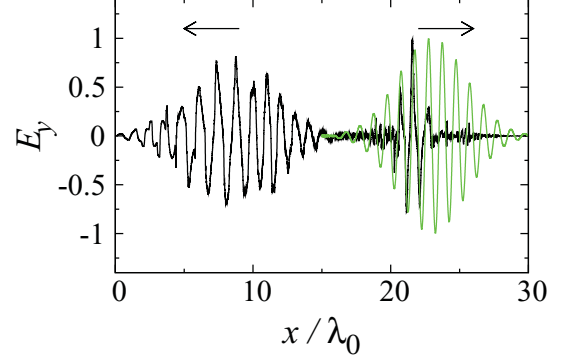

FIG. 3. (Color online) Shapes of the incident laser pulse [green (light gray) line, $a_0 = 20$] and the pulse after interaction with a carbon foil having an initial thickness $d = 1.05\lambda_0$ and $n_0 = 8n_{cr}$ (black line; arrows show the direction of propagation for the parts of this pulse).

increase at $t = 7T_0$ from the beginning of interaction (just when the laser pulse peak enters the plasma layer) and has a maximum of 97% near $t = 9T_0$. As such, the top of the transmission is delayed for more than one period, with respect to the most intensive interaction of the laser pulse with the plasma layer (note that $d = \lambda_0$ for Fig. 1). In other words, the transparent channel exists for two periods of the laser pulse: from $t \sim 8T_0$ to $t \sim 10T_0$. Figure 1(a) shows the shape of the pulse after transmission through the plasma layer. The duration of the transmitted pulse is seen to be nearly single cycle (FWHM is $\sim$4 fs or $1.2T_0$), which is almost 5 times smaller than the FWHM duration of the incident pulse.

From the consideration above, it becomes evident that to ensure that the the transparent channel closes reliably, it is necessary to realize a boundary regime between the anomalous penetration and hole-boring modes by choosing appropriate laser pulse and target parameters. On the other hand, the relation between the laser pulse duration and the time for opening the transmitting window (penetration time) is also important. If the target is too thin, the penetration time is considerably smaller than the laser pulse duration. In this case, the laser pulse is too intense after start of the transmission, and the channel cannot close until the intensity of the laser pulse considerably decreases. This case is shown in Fig. 2(a) ($d = 0.7$ μm), where the generation of a strongly asymmetric pulse with a sharply rising front is presented, in which the peak amplitude can be reached in about one cycle. Here, the mechanism for the sharpening of the laser pulse front is the same as before, but the transmittance window remains open during the whole interaction time (the second scenario for laser pulse shaping). In this case, the tail of the transmitted pulse resembles the tail of the incoming pulse.

The features of shaping considered above can also be realized for heavier ions, e.g., for carbon ions. The transmitted pulse shaped with the carbon target is presented in Fig. 3. Parameters for the shaping are as follows: $a_0 = 20$, $d = 1.05\lambda_0$, and $n_0 = 8n_{cr}$, and the target is considered to be fully preionized. Hence, from Fig. 3, it can be concluded that the shape of the transmitted pulse is very close to that in Fig. 1(a).

B. Characteristics for transmitting window

The characteristics of the transmittance window as functions of the incident amplitudes of the laser pulse and the thickness of the plasma layer are presented in Figs. 2(c) and 2(d). Note that when the amplitude of the pulse increases, the transition from opacity to transparency occurs earlier [Fig. 2(c)]. For the amplitude $a_0 > 22$, the transmission channel is maintained until the end of the interaction. There is no channel formation for the amplitude $a_0 \leqslant 18$. Laser pulses with an amplitude between 18 and 22 have a finite transmission channel, so the transmitted pulse duration is defined by the length of this channel. The transmittance of the plasma layer having different thicknesses is presented in Fig. 2(d) for $a_0 = 20$. Again, there is a threshold thickness $d \sim 1.2$ λ_0, and the range of thicknesses for generating the short pulse is $\lambda_0 < d < 1.2\lambda_0$.

The role of initial electron density of the target is demonstrated in Fig. 4 (proton target). For $n_0 = 8n_{cr}$, the first three periods of the transmitted pulse are similar to those in Fig. 1(a) [note that the dimensionless surface charge density $\alpha = \pi(\omega_p^2/\omega^2)(d/\lambda_0) = 31.4$ in Fig. 1(a), Fig. 4(a), and Fig. 4(b)]. However, for $n_0 = 8n_{cr}$, the transmission channel does not close, and an asymmetric pulse is generated. For $n_0 = 12n_{cr}$, the transmission channel does not open at all. In this case, the hole-boring mode of interaction is realized, and the laser pulse is thus not able to heat the electrons strong enough to reduce the formed peak of the electron density below n_{cr}. To make the target transparent in this case, the laser pulse amplitude has to be considerably increased. For even greater densities, larger laser pulse amplitudes are required, which makes it more difficult to realize in experiments.

Similar features can be obtained for other initial electron densities in the target and laser pulse durations. Short pulses can be generated if the shaping regime is at the boundary between the anomalous penetration mode and hole-boring mode. For a given electron density, this regime corresponds to a relatively narrow interval of laser pulse amplitudes; however, for each electron density, the corresponding amplitude of
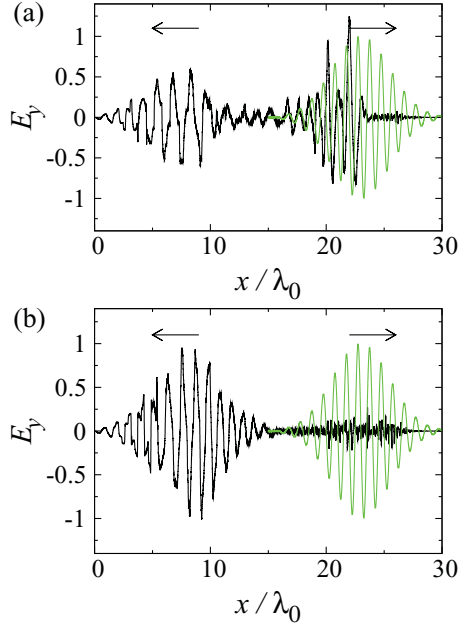
FIG. 4. (Color online) Shapes of the transmitted pulse ($a_0 = 20$) for (a) $n_0 = 8n_{cr}, d = 1.25\lambda_0$ and (b) $n_0 = 12n_{cr}, d = 0.83\lambda_0$. In both cases, $\alpha \simeq 31.4$.
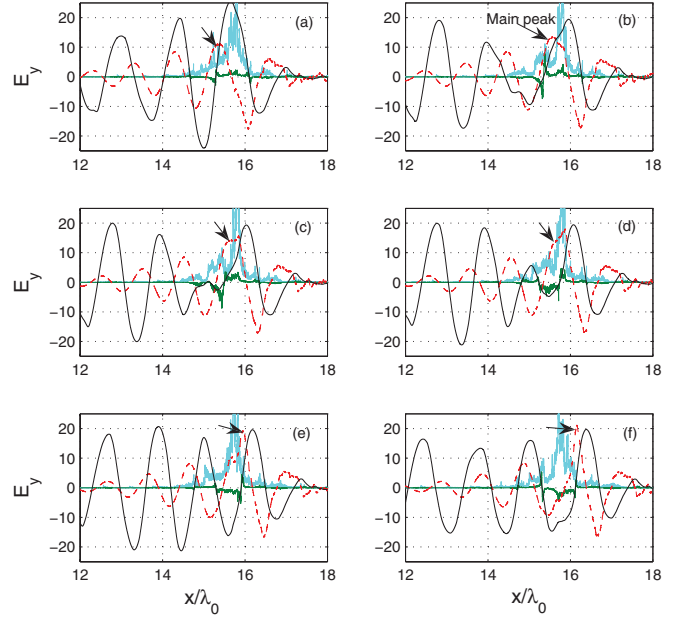

FIG. 5. (Color online) Evolution of the 10th positive half cycle (marked with the black arrows) of the incident laser pulse producing the output half cycle with the maximal amplitude during transmission through the plasma layer (electric field of the right-going wave is shown with the dashed red line): (a) $t = 9.54T_0$, (b) $t = 9.7T_0$, (c) $t = 9.76T_0$, (d) $t = 9.8T_0$, (e) $t = 9.9T_0$, (f) $t = 10.1T_0$. Also, total vector potential (solid black line), electron density [cyan (light gray) line], and instant radiation of the cells to the right [green (dark gray) line] are shown (the radiation field is increased by 15 times). The parameters of the interaction are the same as in Fig. 1.

the pulse, which realizes this regime, can be found. The asymmetric pulses can be generated in either anomalous penetration mode or in hole-boring mode (for relatively long laser pulses with a high enough amplitude).

C. Increased intensity for transmitted pulse

We also found a very interesting effect pertaining to the interaction of a linearly polarized laser pulse with the plasma layer. Due to this effect, the peak intensity of the transmitted pulse can be equal or even higher than the initial laser peak intensity [cf. Fig. 1(a)]. The evolution during transmission through the plasma layer for the 10th positive half cycle of the incident laser pulse [cf. the inset in Fig. 6(b)], which produces the output half cycle with the maximal amplitude, is presented in Fig. 5 (for short, this half cycle is called a main peak below; note that in the incident laser pulse, it is not the peak with the largest amplitude). From this figure, it is clearly evident that the front of the main peak is amplified with the final amplitude almost two times greater than the initial amplitude of this peak, and the rear is depleted, and this process occurs because of the radiation of the electrons. Due to a small thickness of the plasma layer (less than $\lambda_0/2$ after compression), the total transmission takes less than $T_0/2$ for the main peak.

The transformation of the laser pulse intensity envelope during this interaction is presented in Fig. 6(a) and the evolution of the positive half cycle amplitudes is shown in Fig. 6(b) [only for the 8th positive half cycle with the maximal initial amplitude and two positive half cycles after it; cf. the inset in Fig. 6(b)]. At first, the duration and maximal amplitude of the laser pulse decreases then, after the start of transmission, the amplitude increases with an almost constant duration. From Fig. 6, it can be concluded that the part of the laser pulse from the beginning to the maximal amplitude is reflected and absorbed by the target electrons. After the

most intensive part of the laser pulse has passed, the electrons reemit light and thereby increase the transmitted field. As a result, the maximal amplitude of the transmitted pulse is about 16% larger than that for the incident laser pulse, and this maximal amplitude belongs to the half cycle, of which the input amplitude is equal to 13. Also, from simulations, the energy of the input cycle producing the output cycle with the maximal amplitude is 1.9 times smaller than the total energy of the corresponding cycles in transmitted and reflected waves and 1.4 times smaller than the energy of the output cycle with the maximal amplitude. So the process of interaction cannot be represented as a simple transmission of some large-amplitude half cycles of the incident laser pulse through the transparent plasma layer.

The spectrum of the transmitted laser pulse is shown in Fig. 2(b), together with the spectrum of the incident pulse. The figure shows a high level of harmonics, from which the second, third, and fourth harmonics are seen to be the most intense. However, the effect of increasing the intensity of the transmitted pulse cannot be solely related to the generation of harmonics. Indeed, the coherent wake emission mechanism cannot work for the normal incidence of the laser pulse [30]. And the other possible mechanism for generation of harmonics, the relativistic oscillating mirror model, is unable to fully explain the resulting increase of intensity for the transmitted pulse because the target is transparent and has the thickness of about $\lambda_0/2$ at the time of transmission [Fig. 1(d)]. Also, the increase of the cycle-averaged energy of the pulse
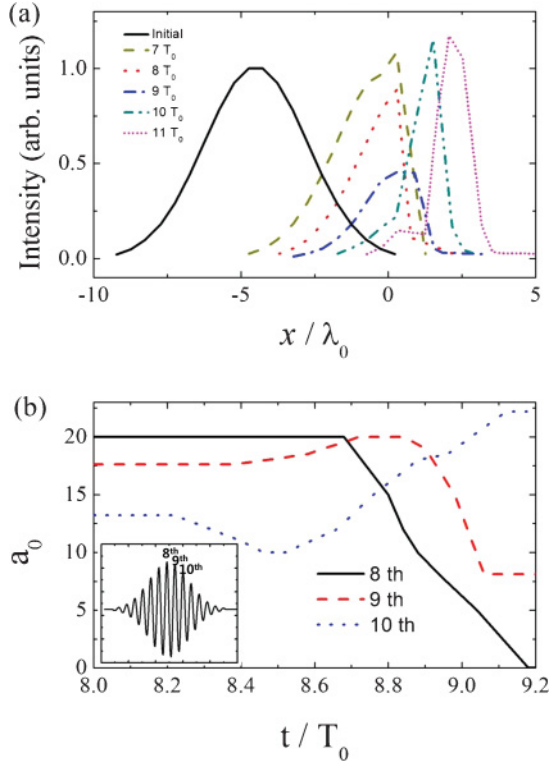
FIG. 6. (Color online) (a) Transformation of the laser pulse intensity envelope during interaction and (b) evolution of the positive half cycle's amplitudes (adjusted in time for easy comparison). Positions of the tested positive half cycles in the input laser pulse are shown in the inset (in the incident laser pulse, the eighth positive half cycle has the largest amplitude). The parameters of the interaction are the same as in Fig. 1.

during transmission indicates that generation of harmonics cannot be the main mechanism for the effect of the amplitude enhancement. The full analytical theory for this effect can be very complicated since several processes have to be taken into account, such as the longitudinal resonance (induced by the oscillating ponderomotive force) of the electrons in the ion field during changes of the effective plasma frequency from $\omega_{pef} \gg \omega_0$ (opacity) to $\omega_{pef} < \omega_0$ (transparency), electrons bunching and radiation in the field of two counterpropagating waves, strong relativistic nonlinearity, the generation of intense harmonics through nonlinear interaction in the presence of the magnetic field of the laser pulse, and others.

One possible model explaining the increased intensity can be as follows. The incoming pulse front pumps the longitudinal oscillations of the electrons, which can store energy for a relatively long time (several laser periods) due to the presence of the Coulomb force created by the ions. The distribution of the electrons over their longitudinal velocity just before transmission of the main peak ($t = 9.2T_0$) is shown in Fig. 7 ($\beta_x = v_l/c$, where v_l is the longitudinal velocity of an electron). This distribution shows that three groups of electrons are present in the layer: The electrons in the first group have relatively low longitudinal velocities, and in the other two groups, the electrons have relativistic velocities, which coincide with or are opposite to the laser pulse propagation direction. The last two groups of electrons
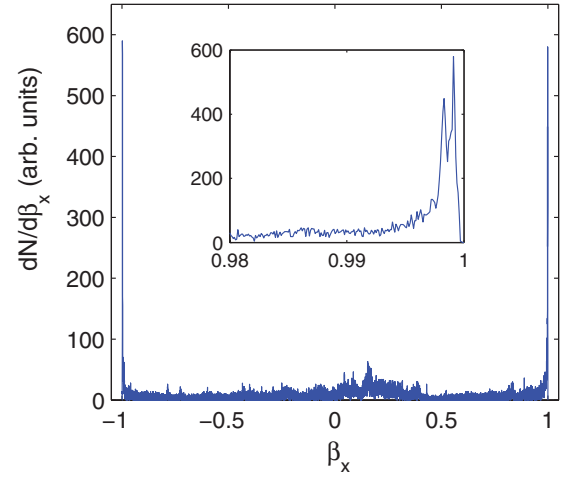

FIG. 7. (Color online) Distribution of the electrons over longitudinal velocity before transmission of the main peak ($t = 9.2T_0$). Inset: zoom of the distribution near $\beta_x \simeq 1$. The parameters of the interaction are the same as in Fig. 1.

provide for intensive longitudinal circulation of the electrons in the layer. The longitudinal motion of the electrons is governed not only by the laser pulse but by the Coulomb forces of the ions as well. Then, if the longitudinal momentum of the electron is considerably greater than mc, its longitudinal velocity $\beta_x = p_x/\sqrt{1 + p_x^2 + p_y^2}$ increases considerably when the transverse momentum p_y becomes small during transmission of the laser pulse (here and below the momenta are normalized with mc). Note that for an electron, which is free and motionless before interaction with an electromagnetic wave, during interaction, transverse and longitudinal momenta tend to zero simultaneously, and there is no increase for the longitudinal velocity at that times. This effect is clearly seen in Fig. 8(b), where the phase spaces $x - \beta_x$ and $x - \beta_y$ for the electrons are presented. The electrons enclosed with a red ellipse near $x \approx 15.3$ have small transverse velocities β_y and ultrarelativistic longitudinal velocities β_x, which are greater than 0.999 for some of them.

In this situation, the ultrarelativistic electrons can interact effectively with the laser half cycle passing the target at this moment of time (note that the thickness of the target at the time of transmission is only about $\lambda_0/2$, so every half cycle interacts with it one after another). The radiation field of an electron (which is an electron sheet in the 1D model) is defined by [13]

$$\mathbf{E}_{\perp\pm}(x,t) = -2\pi\sigma \frac{\boldsymbol{\beta}_\perp(t')}{1 \pm \beta_z(t')}, \qquad (1)$$

where $\mathbf{E}_{\perp\pm}(x,t)$ and $\boldsymbol{\beta}_\perp$ are the radiation and the transverse velocity of the electron sheet (minus and plus signs correspond to the right- and left-going radiation of the sheet correspondingly), t' is the retarded time

$$c(t - t') = |x - \tilde{X}(t')|, \qquad (2)$$

and $\tilde{X}(t')$ is the longitudinal coordinate of the electron sheet. So if an electron has a relativistic longitudinal velocity, the radiation field increases considerably in the direction of this velocity (Doppler effect). In our case, there are electrons with $\beta_x \simeq 1$ and $\beta_x \simeq -1$, while the total number of electrons is
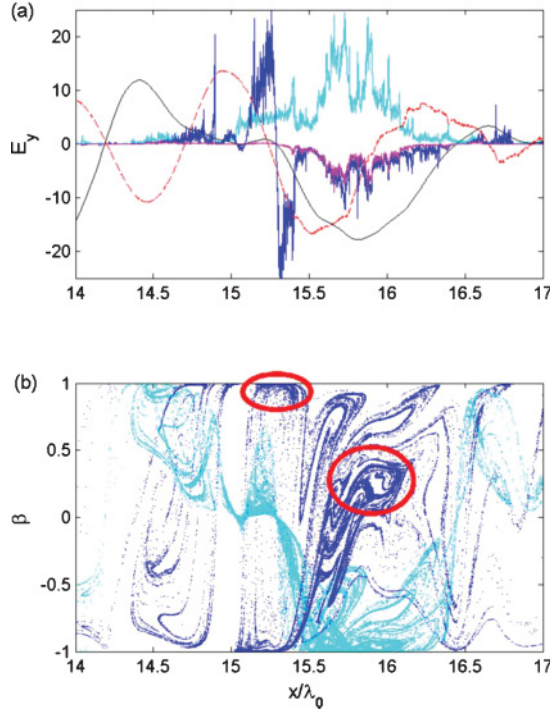
FIG. 8. (Color online) Two sources of electron radiation in the plasma layer at $t = 9.2T_0$. (a) Radiation field of the electron sheets [blue (dark gray) line, increased by 90 times for better visibility], radiation of the same sheets calculated for $\beta_x = 0$ [magenta (medium gray) line, also increased by 90 times], electron density [cyan (light gray) line], vector potential of the standing wave (black line), and electric field of the right-going wave (dashed red line). (b) Phase spaces $x - \beta_x$ [blue (dark gray) line] and $x - \beta_y$ [cyan (light gray) line] for the electrons of the layer. The electrons, which form two radiation sources, are enclosed with ellipses. The parameters of the interaction are the same as in Fig. 1.

fixed. Then, the total right-going radiation of two electron sheets with $\beta_x \simeq 1$ and $\beta_x \simeq -1$ is defined by

$$\mathbf{E}_\perp(x,t) = -2\pi\sigma \left(\frac{\boldsymbol{\beta}_\perp(t')}{1 + \beta_x(t')} + \frac{\boldsymbol{\beta}_\perp(t')}{1 - \beta_x(t')} \right)$$
$$= -4\pi\sigma\boldsymbol{\beta}_\perp(t')\gamma_l^2, \qquad (3)$$

where the longitudinal gamma factor is $\gamma_l = [1 - (v_l/c)^2]^{-1/2}$. When $\gamma_l \gg 1$ the radiation of two electron sheets moving relativistically in the opposite directions along x will be considerably greater than the radiation of two motionless sheets. Since for $\boldsymbol{\beta}_\perp = 0$ the radiation field is equal to zero, the peaks of the radiation field will be positioned near these points, where $\boldsymbol{\beta}_\perp \approx 0$ and $\beta_x \simeq 1$.

The radiation field of the electrons at $t = 9.2T_0$ (just before transmission) is presented in Fig. 8(a) [blue (dark gray) line, increased by 90 times for better visibility] and in Fig. 5 [green (dark gray) line, increased by 15 times]. The radiation of the electron sheets supposing they are motionless along x is also presented in Fig. 8(a) [magenta (medium gray) line, also increased by 90 times]. These radiations were calculated by summation of radiation fields of all electron sheets in some cell obtained from Eq. (1) (note that this is the instant radiation and it does not equal the total radiation of the plasma layer at $t = 9.2T_0$). From Fig. 8(a), one can conclude that, generally,

there are two sources producing high-amplitude radiation. One source of radiation is formed in the region, where the electron density is maximal [radiation of the electrons from $x \simeq 15.7$ to $x \simeq 16$ in Fig. 8, also marked with the red ellipse in Fig. 8(b)]. This source is motionless along x (or moves slowly as a whole with the ion velocity) so the role of the longitudinal velocity is not very important here [the radiation field of this source is approximately equal to the radiation of the same sheets calculated for $\beta_x = 0$; cf. blue (dark gray) and magenta (medium gray) lines in Fig. 8(a)]. Because of the very small dimensions of the radiation source (less than $\lambda_0/2$), it can radiate coherently.

The second radiation source is formed by the electron sheets, which are near the point where $\beta_y \approx 0$ and $\beta_x \approx 1$ (from $x \simeq 15.2$ to $x \simeq 15.4$ in Fig. 8). Here, the role of the longitudinal velocity is very important, and the radiation field of this source is considerably greater than the radiation of the same sheets calculated for $\beta_x = 0$ [cf. blue (dark gray) and magenta (medium gray) lines in Fig. 8(a) near point $x = 15.3$]. The maximal amplitude of the radiation of this source can be comparable to or even larger than the maximal amplitude of the first source radiation in spite of the smaller electron density. Usually, the dimension of this source is considerably smaller than the dimension of the first source, so it can also radiate coherently.

Because of conservation of the transverse component for generalized momentum, the dimensionless transverse momentum of each electron is equal to a total vector potential A (normalized by mc^2/e) of a standing wave formed by the right-going and reflected waves estimated at the position of this electron. So the position of each point where $A = 0$ and $\beta_y = 0$ is defined by the vector potential solely and, thus, the radiations of all electrons near this point have the same phase, which is determined by the vector potential [in spite of different longitudinal velocities of the electrons; cf. blue and black lines in Fig. 8(a)]. Before transmission, the points of $A = 0$ move slowly to the right because the reflected wave has a decreased frequency (due to acceleration of ions and slow motion of the boundary). In this case, the radiation field of such a point cannot sum up coherently and grow in time so the amplitude of the total radiation is small. When transmission starts, the structure of the field changes, and the reflection of the plasma layer decreases considerably. The radiation of the first source is permitted to go out of the plasma layer. Also, after start of transmission, the points of $A = 0$ inside the plasma layer start to move together with the right-going wave so the radiation sums up coherently in time and the wave increases during propagation. When the radiations of two sources add in phase the amplitude of the transmitted wave increases as in Fig. 5. At the interface of the standing and right-going waves of the vector potential, an additional cycle is formed every half period as can be seen in Figs. 5(c) and 5(d). The additional points of $A = 0$ modify the radiation field of the electrons and affect the propagation of the wave forming the output structure of the field.

So the energy of longitudinal oscillations can be reverted back into the transverse field due to coherent electron radiation. This model is supported also by the time dependence of the averaged energy γ_{lav} stored in the longitudinal motion of the electrons. Before opening the transmitting window, γ_l
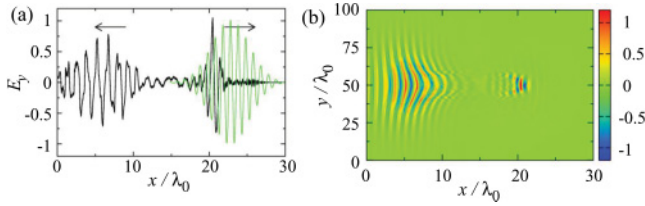
FIG. 9. (Color online) (a) The transverse field from 2D PIC simulations at $y/\lambda_0 = 50$. (b) Pulse shapes for $d = 1.7\lambda_0$, $n_0 = 10 n_{cr}$, $a_0 = 20$, and a spot size (FWHM) of $23.5\lambda_0$.

increases, then during high transmittance, it decreases; after closing the transmitting window, it increases again [dashed blue line in Fig. 1(b)].

It is also interesting to note that the maximum of the transmitted pulse spectrum is shifted to a higher frequency with respect to the maximum of the incident pulse spectrum (by 7%), which corresponds to the velocity of the laser pulse front during the start of the transmission. Accordingly, the third harmonic has maximum at about $3.22\omega_0$. This occurs because the radiation of the plasma layer is synchronized by the vector potential, the spatial structure of which forms inside the layer and moves together with it.

D. 2D PIC simulations for shaping laser pulses having linear polarization

We performed 2D PIC simulations to investigate the effects of higher dimensions. For this task, a simulation box having dimensions of $30\lambda_0$ along the x direction and $100\lambda_0$ along the y direction was used. The size of the grid mesh was $(\lambda_0/100) \times (\lambda_0/50)$. Here, a linearly y-polarized laser pulse with a Gaussian envelope was used for propagation along the x axis. The pulse duration was $\tau_l = 5.83$ at FWHM, the peak amplitude was $a_0 = 20$, the FWHM intensity spot size was $23.5\lambda_0$, and the incidence was normal. Here, a plasma layer with density of $n_0 = 10 n_{cr}$ was located from $15\lambda_0$ to $16.7\lambda_0$. Note that we used a thicker plasma layer to account for deformation of the foil caused by the 2D hole-boring process. As seen in Fig. 9(a), the FWHM duration of the transmitted pulse is about 4 fs ($1.2T_0$), which is almost identical to the 1D case. The transverse FWHM spot size of the transmitted pulse is $6\lambda_0$, which is about four times smaller than the incident spot size. The maximal amplitude of the transmitted pulse is 10% larger than that for the incident laser pulse. Therefore, we could also confirm the increase of amplitude for the 2D case.

Similar results were obtained for the shaping laser pulses having an FWHM spot size of $12\lambda_0$, interacting with a foil having the same thickness, $d = 1.7\lambda_0$. For smaller spot sizes, a decrease of the foil thickness might be necessary to recover the same results for shaping.

III. SHAPING CIRCULARLY POLARIZED LASER PULSES

For shaping circularly polarized laser pulses, distributions of the electron density are regular and very different from those of linearly polarized laser pulses [Figs. 10(c) and 10(d)]. For circular polarizations, the ponderomotive force acts only in the forward direction such that the heating of the electrons is almost suppressed; therefore, this case can be referred
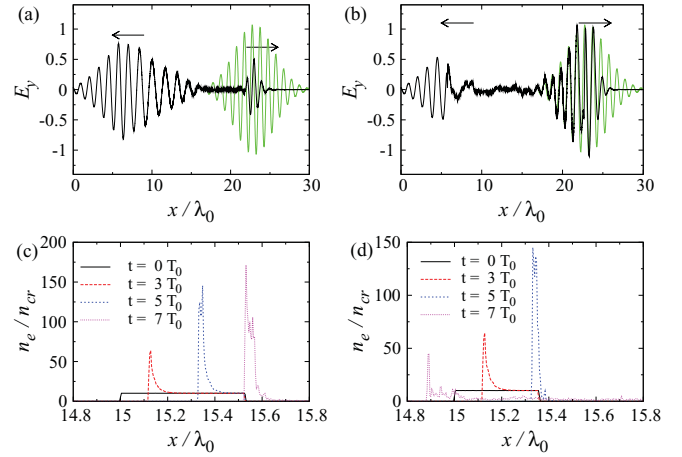

FIG. 10. (Color online) Shapes of the incident laser pulse with circular polarization [green (light gray) line, $a_0 = 20$] and the pulse after interaction with plasma layers having an initial thickness of (a) $d = 0.53\lambda_0$ and (b) $d = 0.36\lambda_0$ (solid black lines, arrows show the direction of the propagation for parts of this pulse, $n_0 = 10 n_{cr}$). Also shown are the distributions of electron density for different times for (c) $d = 0.53\lambda_0$ and (d) $d = 0.36\lambda_0$.

to as dynamic shaping. During this interaction, the plasma layer can be compressed to about a skin depth. Concurrently, due to the relativistic increase of the electrons' mass in the plasma layer, the effective skin depth increases. Then, when the skin depth becomes larger than the compressed thickness of the plasma layer, transmission begins and lasts until there is a decrease in the intensity of the incident laser pulse and a corresponding decrease of the effective skin depth. For this reason, the transmitted pulse can be considerably shorter than the incident pulse [23], as shown in Fig. 10(a). After compression of the electrons, the process of shaping becomes very similar to that for ultrathin foils, as described by the flying mirror model [13]. Indeed, full compression (and correspondingly, high transmission) is possible only when the laser pulse amplitude becomes greater than the parameter α (the part of the pulse above the line for α in Fig. 11), so, automatically, before achieving transmission, the plasma layer has to be compressed to the thickness of an ultrathin foil, and this is the range of validity for the flying mirror model. Predicted envelopes of the transmitted pulse from this model are presented in Fig. 11 ($d = 0.53\lambda_0$, $a_0 = 20$, and $\alpha = 16.64$). Note that the numerical solution from the flying mirror model [red (dashed) line; Eq. (23) of Ref. [13] generalized for the circular polarization] indicates that the asymmetry of the envelope is similar to the asymmetry of the pulse from the PIC simulations. The analytical solution [light green (dotted) line; Eq. (26) of Ref. [13]], though symmetrical, allows us to obtain simple estimates for parameters of the transmitted pulse. Therefore, it can be inferred that this model gives a reasonable description of the shaping process. As such, the increased duration of the predicted envelope can be explained by the stronger suppression of the pulse front by the plasma layer (in contrast to the ultrathin foil) and by the motion of ions (not accounted for in the flying mirror model).

A circularly polarized pulse with a sharp rising front (peak amplitude is reached at nearly one cycle) can be
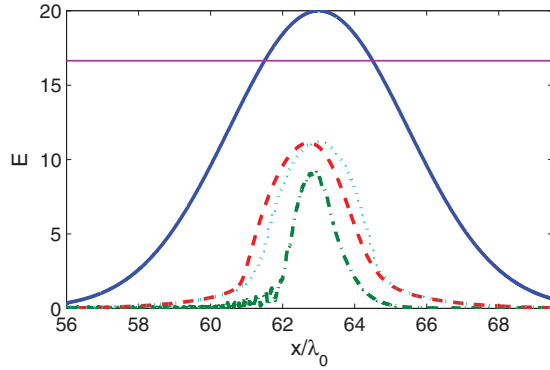
FIG. 11. (Color online) Envelopes for the transmitted pulse predicted via the numerical (dashed red line) and analytical (dotted light green line) solutions of the flying mirror model for $a_0 = 20$ and $d = 0.53\lambda_0$. The envelopes of the incident pulse (solid blue line) and the transmitted pulse from the PIC simulations at $t = 43T_0$ (dashed-dotted green line) are also shown for comparison. The value of α is indicated by the horizontal solid magenta line.

also produced during shaping with a sufficiently thin plasma layer [Fig. 10(b)]. The shaping process for the front of the transmitted pulse here is very similar to that for the short transmitted pulse. However, at some threshold amplitude, the foil is destroyed abruptly [Fig. 10(d) for $t = 7T_0$]. After destruction, the electrons return to their ions and the electron density greatly decreases such that the amplitude of the transmitted asymmetric pulse is about that of the incident one. Also, due to longitudinal oscillations of the electrons after destruction of the foil, one can find here some features which are typical for the shaping of the linearly polarized laser pulses (e.g., the amplitudes of some half cycles in the transmitted pulse can be larger than the maximal amplitude of the incident pulse).

IV. DISCUSSION OF RESULTS AND CONCLUSIONS

Although the transmission mechanisms are different for linear and circular polarizations, two types of transmitted pulses (nearly one cycle and strongly asymmetric) can be generated for both cases by changing only the thicknesses of the plasma layer. For short transmitted pulses, the amplitude for the circular polarization is about two times smaller than the amplitude for the linear polarization; at the same time, both amplitudes have similar values for strongly asymmetric pulses. Also, in the linear polarization case, strong harmonics are generated, whereas for the circular polarization the intensity of harmonics is very small [Fig. 2(b)]. For the shaping of circularly polarized laser pulses, the amplitude of the incident pulse should be larger than the value of parameter α for the foil. In this case only can the amplitude of the transmitted pulse be considered reasonable. For linearly polarized laser

pulses, parameter α does not play such a crucial role; i.e., the amplitude of the incident pulse can be smaller than α and good shaping is still possible (cf. Fig. 1).

For a practical realization of the shaping procedure described above, relatively low densities of the target are necessary, $n_0 \sim (10$–$20)n_{cr}$. These densities can be produced in principle via a special preparation of the target. First, a laser pulse of a subrelativistic intensity should interact with a nanofilm target. This interaction will warm the electrons in the target, thereby expanding the target and reducing the electron density. Then, after some time, the main laser pulse can be launched at the target. Such a preparation for the target can also be performed with a controlled prepulse from the main laser pulse. To facilitate the adjustment of the laser pulse amplitude with the electron density of the produced plasma layer, it is possible to change in experiment the amplitude of the main laser pulse (e.g., by defocusing or decompression) keeping the electron density constant (i.e., with the same preparation procedure for the target) until achieving the desired result for the laser pulse shaping.

The shaping of the laser pulses with thin films is likely to be the most effective for a super-Gaussian transverse-shaped laser pulse. In this case, the power of the transmitted pulse will be maximal. Also, for super-Gaussian laser pulses, the spatial fluctuations of the amplitude in the focal spot will be decreased, as modern petawatt-class laser installations offer the possibility for generating flat-top laser pulses with field amplitude fluctuations of less than 6.5% in the laser spot [31], achieved via the nonlinear processing of the pulse inside the system.

In summary, we have shown that petawatt-class laser pulses with nearly single-cycle duration or with a strongly asymmetric longitudinal profile can be generated using a thin plasma layer. In this study, a new effect was found for the shaping of linearly polarized laser pulses. Owing to this effect, the peak amplitude of the transmitted pulse can be not smaller than that of the incoming pulse (and even larger), which is very important for numerous applications. For the shaping laser pulses having circular polarization, it was also shown that the flying mirror model can be effectively used to predict the shape of the transmitted pulse.

[1] V. A. Vshivkov *et al.*, Phys. Plasmas **5**, 2727 (1998).

[2] S. Guérin *et al.*, Phys. Plasmas **3**, 2693 (1996).

[3] K. Nagashima, Y. Kishimoto, and H. Takuma, Phys. Rev. E **58**, 4937 (1998).

[4] R. A. Cairns, B. Rau, and M. Airila, Phys. Plasmas **7**, 3736 (2000).

[5] J. Fuchs *et al.*, Phys. Plasmas **6**, 2569 (1999).

[6] U. Teubner, Phys. Rev. Lett. **92**, 185001 (2004).

[7] V. V. Kulagin *et al.*, Appl. Phys. Lett. **85**, 3322 (2004).

[8] V. V. Kulagin *et al.*, Phys. Plasmas **11**, 5239 (2004).

[9] V. V. Kulagin, V. A. Cherepenin, Y. V. Gulyaev, V. N. Kornienko, K. H. Pae, V. V. Valuev, J. Lee, and H. Suk, Phys. Rev. E **80**, 016404 (2009).

[10] V. V. Kulagin, V. A. Cherepenin, M. S. Hur, and H. Suk, Phys. Rev. Lett. **99**, 124801 (2007).

[11] A. Henig *et al.*, Phys. Rev. Lett. **103**, 045002 (2009).

[12] S. Bulanov, IEEE Trans. Plasma Sci. **24**, 393 (1996).

[13] V. V. Kulagin, V. A. Cherepenin, M. S. Hur, and H. Suk, Phys. Plasmas **14**, 113102 (2007).

[14] G. D. Tsakiris *et al.*, New J. Phys. **8**, 19 (2006).

[15] K. Schmid *et al.*, Phys. Rev. Lett. **102**, 124801 (2009).

[16] P. Kaw and J. Dawson, Phys. Fluids **13**, 472 (1970).

[17] M. Tushentsov, A. Kim, F. Cattani, D. Anderson, and M. Lisak, Phys. Rev. Lett. **87**, 275002 (2001).

[18] E. Lefebvre and G. Bonnaud, Phys. Rev. Lett. **74**, 2002 (1995).

[19] B. Shen and Z. Xu, Phys. Rev. E **64**, 056406 (2001).

[20] V. Goloviznin *et al.*, Phys. Plasmas **7**, 1564 (2000).

[21] F. Cattani, A. Kim, D. Anderson, and M. Lisak, Phys. Rev. E **62**, 1234 (2000).

[22] V. I. Eremin, A. V. Korzhimanov, and A. V. Kim, Phys. Plasmas **17**, 043102 (2010).

[23] L. L. Ji, B. F. Shen, X. M. Zhang, F. C. Wang, Z. Y. Jin, C. Q. Xia, M. Wen, W. P. Wang, J. C. Xu, and M. Y. Yu, Phys. Rev. Lett. **103**, 215005 (2009).

[24] D. Bauer, R. R. E. Salomaa, and P. Mulser, Phys. Rev. E **58**, 2436 (1998).

[25] F. Tavella *et al.*, Opt. Lett. **32**, 2227 (2007).

[26] J. P. Verboncoeur *et al.*, Comput. Phys. Commun. **87**, 199 (1995).

[27] H. Sakagami and K. Mima, Phys. Rev. E **54**, 1870 (1996).

[28] S. C. Wilks, W. L. Kruer, M. Tabak, and A. B. Langdon, Phys. Rev. Lett. **69**, 1383 (1992).

[29] T. Schlegel, N. Naumova, V. T. Tikhonchuk, C. Labaune, I. V. Sokolov, and G. Mourou, Phys. Plasmas **16**, 083103 (2009).

[30] C. Thaury and F. Quéré, J. Phys. B **43**, 213001 (2010).

[31] J. H. Sung *et al.*, Opt. Lett. **35**, 3021 (2010).